Powder Materials in Industry

Bibliography

Prepared by
Fawzia Al-Buloushi

KUWAIT INSTITUTE FOR SCIENTIFIC RESEARCH

NATIONAL SCIENTIFIC & TECHNICAL INFORMATION CENTER

TECHNICAL SERVICES DEPARTMENT

July 2022

Table of Content

Introduction

The technology of utilizing metal powders, offers the engineer a means conserving materials, reducing machining and securing a uniform product at a reasonable cost. This unique metal-forming method permits the production of parts with close tolerances and a minimum of scrap. It also enables the development of products that cannot be produced by any other method. By proper selection of powders, the powder metallurgy (P/M) specialist can control the density of products over a wide range and secure a wide range of mechanical and physical properties. He can produce mixtures of metals that are insoluble in each other or mixtures of metals and nonmetals that combine the properties of both.

Density can be controlled to produce parts with porosities as high as 60%, or conversely, those that are practically pore-free and have densities approaching the theoretical density of the metal. It is also possible to vary the density in a single part. And by producing parts with interconnected pores, the metallurgist can obtain a skeleton that can be impregnated with oils, plastics or even a metal having a lower melting point.

This Bibliography is a search from 2021-2022

Title: Multi-objective Optimization of EDM and Powder Mixed EDM for H-11 Steel

Author: Tripathy, S., Tripathy, D.K.

Source: 2023 Lecture Notes in Mechanical Engineering

pp. 689-698

Abstract:

Electrical discharge machining (EDM) is a benchmark method for material removal from workpiece in aerospace, automotive, dies and mold making industries, etc. To enhance the process performance of EDM, powder mixed electrical discharge machining (PMEDM) is being expansively put to use by practitioners for improving the performance of the process while maximizing the efficiency and enhancing the quality of the surface. The present study aims at investigating the influence of "concentration of powder (Cp), peak current (Ip), on time of spark (Ton), duty cycle (DC), and gap voltage (Vg) on responses like rate of material removal (MRR), rate of tool wear (TWR), wear ratio of the electrode (EWR), and roughness of the surface (SR)" for EDM and PMEDM of H-11. Taguchi's experimental design technique is used along with technique for order of preference by similarity to ideal solution (TOPSIS) followed by gray relational analysis (GRA) to estimate the performance of the process. Graphite powder of size less than 53 µm has been used as the additive for experiments conducted with L27 orthogonal array. Electrolytic copper has been taken as the tool electrode for conducting the experiments. An improvement of 0.115631 and 0.14211 in preference value is observed while conducting the confirmatory experiments with the use of TOPSIS and GRA. The optimal set of input parameters from TOPSIS is achieved at Cp = 6 g/l, Ip = 3 A, Ton = 200 µs, DC = 80%, and Vg = 50 V and from GRA as Cp = 6 g/l, Ip = 3 A, Ton = 150 µs, DC = 80%, and Vg = 30 V.

Title: Fresh and Mechanical Properties of One-Part Alkali-Activated Self-Consolidating Concrete

Author: Kanaan, D.M., Soliman, A.M.

Source: 2023 Lecture Notes in Civil Engineering

240, pp. 17-30

Abstract:

There is a significant potential for Alkali-activated self-consolidating concrete (AASCC) to be used in the construction industry. AASCC combines the benefits of both self-consolidating concrete (SCC) and sustainable development. The aim of this study was to develop an experimental program to

investigate the potential production of one-part AASCCs mixtures of multi precursor dry-powder activator materials. Concrete mixtures are developed by incorporating different dosages (16%, 20%, and 25%) of dry-powder activators. The influences of activator dosages on the fresh (slump flow, L-box passing ability, and segregation index) and mechanical properties are critically assessed in terms of experimental findings. Results showed that the workability properties of AASCC highly depended on the dosages of the dry-powder activators. Also, results indicated an improvement in the mechanical properties as the dry-powder activator dosage increased. The findings of this study confirmed the potential for producing one-part AASCC with adequate workability and strength through adjusting activator dosage.

Title: Influence of Zirconia Percent on Physical Properties of Zirconia - Aluminum Chip Matrix (Al6061) Nanocomposites

Author: Al-Alimi, S.A.M., Lajis, M.A.B., Shamsudin, S.B., Long, C.B.

Source: 2022 Journal of Nanostructures

12(1), pp. 194-203

Abstract:

This research intends to propose a new approach to improve the performance of aluminum composites made of chips with the addition of ZrO2 nanoparticles. Moreover, the chip-based composite-reinforced ZrO2 contents offer alternative sources to manufacturing automotive industries to recycle, reuse the machined materials as a secondary source of metal, and protect our earth from greenhouse gas for a sustainable life. This study focused on examining the effects of preheating time (t), preheating temperature (T), and volume fraction (VF) on the mechanical and physical properties of a ZrO2 aluminum chips nanocomposite. This nanocomposite was produced through the hot extrusion method followed by ECAP to compare the result with heat treatment. The influence of each factor was analyzed using the factorial design, followed by RSM. The microstructure and the average grain sizes of the extradites were also investigated. Direct solid states, such as hot extrusion and equal channel angular pressing (ECAP), are alternative and efficient solid-state processes for use in recycling aluminum scrap. These processes utilize less energy and are eco-friendly. Ceramic nanoparticles such as ZrO2 are suggested as alternatives in the production of metal composites. This study investigated and optimized the effects of various parameters of reinforced ZrO2 nanoparticles on the mechanical and physical properties via response surface methodology (RSM). In this study, the nanocomposites made of aluminum AA6061 chips reinforced with 5%, 10%, and 15% volume fraction of ZrO2 powder were produced under different processing temperature of 450°C, 500°C and 550°C. The experimental results were analyzed using the design and analysis of experiments (DOE) principle, and assisted by the Minitab 18 software. It was reported that the maximum yield strength and hardness increased to 119.26 MPa and 65.25 VH compared to 100.26 MPa and 50 VH (as-received AA6061), respectively.

Title: The chemical suitability for recycling of zinc contaminated steelmaking by-product dusts: The case of the UK steel plant

Author: Stewart, D.J.C., Scrimshire, A., Thomson, D., Bingham, P.A., Barron, A.R.

Source: 2022 Resources, Conservation and Recycling Advances

14,200073

Abstract:

Basic oxygen steelmaking (BOS) dust and blast furnace (BF) dust from former and operating steelmaking facilities in the United Kingdom have been characterized by MP-AES, SEM-EDX, particle size analysis, TGA-DSC, combustion analysis, 57Fe Mössbauer spectroscopy, and powder XRD. These materials are a potentially valuable source of Fe for ironmaking, but their contamination with zinc precludes their recycling via the conventional sinter plant/BF route. XRD suggested some of the zinc present in the material is in the form of sub-stoichiometric zinc ferrites ZnxFe3-xO4, making hydrometallurgical separation less effective. BF dust contains 40 wt.% levels of fixed carbon (Cfix) indicating it could be useful as an alternative reductant in rotary hearth furnace processes such as FASTMET. The rotary hearth furnace appears to be the most suited separation technique available due to its lack of sensitivity to zinc present in zinc ferrite compounds, and reintegration of the recovered iron into the steelmaking process.

Title: Powder ageing of Polyamide 6 in laser sintering and its effects on powder and component characteristics

Author: Stiller, T., Berer, M., Katta, A.D.K., (...), Pinter, G., Lackner, J.M.

Source: 2022 Additive Manufacturing

58,102987

Abstract:

The increasing importance of Laser Sintering (LS) for the industry brings a rising number of available materials for this process. One example is the enhanced use of alternative polyamide types like polyamide 6 (PA 6). For polyamide 12 (PA 12), the powder ageing effect is well-known and of great importance from an economical point of view. However, relatively little is known about the powder ageing behavior of newer LS materials. Hence this paper focuses on the experimental powder ageing study of PA 6 in the LS process, both on powder and part level. The powder was reused in total seven times without refreshing and constant sinter parameters were used to produce the samples. Morphological, thermal and rheological measurements of the powder showed a rising number of agglomerates, an apparent increase in the powder crystallinity, and an increase in the viscosity by a factor of 7. These increases consequently affected the density and the mechanical properties of the

parts, latter were determined by tensile tests. Between the first and the last iteration, a decrease of the Young's Modulus of 60 % and the tensile strength of 70 % was observed. Besides the decline of mechanical properties, the geometrical dimensions of the last iteration were only 60 % of the first iteration, the mass was halved and the surface quality suffered from the orange peel effect. The results prove that similar powder ageing effects known for PA 12, and here especially the polyamide post condensation, also take place in LS printing of PA 6.

Title: Development and characterization of sustainable PLA/Olive wood waste composites for rehabilitation applications using Fused Filament Fabrication (FFF)

Author: Fico, D., Rizzo, D., De Carolis, V., (...), Palumbo, E., Corcione, C.E.

Source: 2022 Journal of Building Engineering

56,104673

Abstract:

An understanding of how the construction industry can support the transition towards a Circular Economy (CE) of the built environment plays a key role in rehabilitation processes that often require skilled labor. Fused Filament Fabrication (FFF), an Additive Manufacturing (AM) technique, is a new technology recently proposed for this purpose. In recent years, a number of studies have been presented to improve the sustainability of the main materials used in 3D printing (e.g. PLA filament), suggesting, in particular, some interesting composite filaments. The present paper is related to the development and characterization of sustainable materials, able to reduce the environmental impacts of the conventional materials for FFF. More specifically, various composite filaments based on polylactic acid (PLA) and different amounts of olive wood scraps were produced by an extrusion process and fully characterized from a physical, thermal and mechanical point of view. As they are suitable for application in a low-cost 3D printing machine, these filaments are used to build simple 3D printed models as a first exploitation of architectural building elements based on wood powder. In addition, in order to evaluate the environmental advantages of the wood waste derived composite filaments, the impact indicators were also quantified by Life Cycle Assessment (LCA). LCA results showed environmental benefits resulting from the inclusion of wood scraps in PLA filaments (20% of wood corresponds to 10% impact reduction) supporting further research in this area.

Title: Effects of the sintering temperature on the superior cryogenic toughness of ultra-high molecular weight polyethylene (UHMWPE)

Author: Sui, Y., Li, J., Qiu, Z., (...), Ye, H., Zhou, Q.

Source: 2022 Chemical Engineering Journal

444,136366

Abstract:

Higher requirements for the performance of cryogenic materials bring new challenges to the design and preparation of cryogenic materials. Fortunately, ultra-high molecular weight polyethylene (UHMWPE) displays the potential to become the next generation of cryogenic materials due to its many superior properties, especially its outstanding toughness. In this study, we sintered UHMWPE powders under different sintering temperatures and found that higher sintering temperatures could lead to the final product having better toughness. Surprisingly, the impact strength at −196 °C of UHMWPE sintered at 220 °C is approximately 4.2 times that of polychlorotrifluoroethylene (PCTFE), whose low-temperature impact performance is almost the best among the existing engineering plastics. The maximum cryogenic tensile strength is 158.6 MPa for sintered UHMWPE, while that of PCTFE is only 117.8 MPa. We attributed such outstanding cryogenic toughness to many chain entanglements and proposed a potential mechanism based on scanning electron microscopy (SEM), dynamic mechanical analysis (DMA), differential scanning calorimeter (DSC), and X-ray scattering diffraction (XRD) characterizations. In summary, sintered-mould UHMWPE can be a cost-effective candidate for cryogenic materials in industry due to its superior impact resistance even at −196 °C and other excellent mechanical properties.

Title: Recycling of granite powder and waste marble produced from stone processing for the preparation of architectural glass–ceramic

Author: Luo, Y., Bao, S., Zhang, Y.

Source: 2022 Construction and Building Materials

346,128408

Abstract:

A large amount of solid waste is generated during the stone processing, and a serious environmental issues has arisen from the accumulation of these wastes. In this work, granite powder and waste marble are used to prepare architectural glass–ceramic. The mechanical properties, microstructure, and acid resistance of glass-ceramics designed with different compositions were investigated. With the increase of waste marble content, the main crystalline phase of glass–ceramic changed from anorthite to wollastonite, and the flexural strength of glass–ceramic was also enhanced. When the mass ratio of granite powder to waste marble is 40:60, a CaO-Al2O3-SiO2 (CAS) glass–ceramic with a flexural strength of 109.33 MPa and a Vickers hardness of 6.61 GPa is obtained. After the addition of MgO, the main crystalline phase of the glass–ceramic is augite. Under the addition of 5 wt% MgO, the flexural strength and Vickers hardness of CaO-MgO-Al2O3-SiO2 (CMAS) glass–ceramic reached the maximum, which are 146.95 MPa and 10.24 GPa, respectively. The mechanical properties of these two types of glass-ceramics developed from granite powder and waste marble can

meet the requirements of building materials. From the acid resistance test results, it was found that the higher the content of MgO and CaO in the chemical composition of glass–ceramic, the worse the acid resistance. Therefore, the basic oxide content should be carefully controlled in the composition design of glass–ceramic. This technology of converting granite powder and waste marble into value-added glass–ceramic provides a promising method for the utilization of solid waste from stone processing, which can greatly improve the sustainability of the stone industry.

Title: Photocatalytic performance of N–TiO2@SiO2 composite obtained under gliding arc plasma processing at atmospheric pressure

Author: Suzie, V.A., Jean-Baptiste, T., Elie, A., (...), Georges, K.Y., Samuel, L.

Source: 2022 Results in Engineering

15,100516

Abstract:

Photo catalysis is becoming ubiquitous in the chemical industry because of its positive impact on the cost of operations. Nevertheless, a good photo catalyst must meet the properties of good reactivity, high selectivity, long-term stability, low toxicity, and cost-effectiveness but should also promote a photo-generated charge carriers separation. In this work, a homemade supported catalyst is obtained through low-temperature plasma exposure of the precursor TiCl3/glass powder to promote better handling, high particle dispersion, and easy recovery. Because such a plasma is a strongly oxidative medium containing mainly radicals (•OH and NO•), the mixture exposition induces the formation of N–TiO2 nanoparticles immobilized in-situ onto the glass matrix to form a photo-active hetero-structure that improves the charge carriers' separation overcoming the rapid recombination drawback. The resulting material was characterized by XRD, FTIR, and SEM techniques. The resilient stability after 5 successive cycles, makes this composite a promising alternative photo catalyst for various applications. The photocatalytic degradation yields reached 52, 72, 60, and 80% within 1 h of plasma irradiation and 45, 43, 22, and 25% after 6 h of daylight illumination, respectively for Rhodamine 6G, Floxina B, Ceftriaxone, and Ampicillin. The discrepancy in degradation yields is more related to the intrinsic chemical structure of each contaminant.

Title: Investigation on the potential effects of laser stitching and subsequent heat treatment on the microstructure and mechanical properties of Nickel Alloy 718 produced via Laser Powder Bed Fusion (L-PBF)

Author: Rindler, J.J., Slone, C.E., Herderick, E.D., Mills, M.J., Ramirez, A.J.

Source: 2022 Additive Manufacturing

57,102906

Abstract:

The desire to industrialize and expand the envelope of L-PBF additive manufacturing has driven development of Multi-Laser Powder Bed Fusion (ML-PBF) technology. Stitching of large parts by multiple lasers has become a reality, but the material effects have yet to be well understood. This study examines the differences in mechanical properties and microstructures for stitched and nominal, single laser exposed zones in Nickel-base alloy 718 produced via L-PBF. Multiple industry-relevant heat treatments were examined including stress relief, hot isostatic pressing (HIP), solution heat treatment, and aging. A range of responses between the stitched and nominal zones with each heat treatment have been determined. The addition of an 1120 °C HIP cycle eliminated most signs of heterogeneity between the two zones and provides a promising avenue for industrial adoption.

Title: Use of AFM topography images to determine microindentation hardness of cast tungsten carbide powders

Author: Ciurans-Oset, M., Mundó-Tijeras, I., Mouzon, J., Akhtar, F.

Source: 2022 International Journal of Refractory Metals and Hard Materials

107,105878

Abstract:

Hardness is defined as the resistance of a material to localized plastic deformation. Owing to their non-destructive nature, static indentation hardness tests are widely used in industry. Hardness testing is particularly useful for the mechanical characterization of materials that cannot be tested otherwise, e.g. powdered materials. In this study, challenges related to Vickers micro-indentation hardness testing of hard brittle cast tungsten carbide (CTC) powders were extensively investigated. Test load was optimized to obtain sufficiently large crack-free indentations allowing for precise measurement of the diagonal lengths. The influence of the operator and imaging technique on the measured hardness value was evaluated. Topography of residual imprints was investigated using atomic force microscopy (AFM) and a systematic and operator bias-free method to locate the indentation vertexes was developed. Results suggested that measurement variability introduced by AFM scanning and post-processing was as low as 3.1% and 1.3% with respect to the mean hardness value, respectively. Since the variability due to the measuring system can be isolated, the homogeneity of powders can be reliably evaluated from the hardness measurements thus obtained.

Title: A review of the alumina production from coal fly ash, with a focus in Russia

Author: Valeev, D., Bobylev, P., Osokin, N., (...), Salazar-Concha, C., Verichev, K.

Source: 2022 Journal of Cleaner Production

363,132360

Abstract:

Coal combustion used by the Combined heat and power plants (CHPs) generates solid wastes - coal fly ash (CFA). Up to 22% of the total electricity supply in Russian is coal-generated, this value is forecasted to not decrease until 2035, which in the next 14 years will translate into the accumulation of more than 260 Mt of CFA on the CHPs landfills. Following the Government recently presenting a roadmap towards the ramp-up of the CFA utilization from the current 8%–50% by 2035, the highly developed aluminum industry in Russia amidst the lack of its own bauxite sources is currently considering the utilization of CFA as an aluminum oxide-rich raw material for the alumina production. The present review localizes the largest sources of CFA in Russia, summarizes the annual CFA accumulation rates, and its stored volumes, and the chemical composition of the CFA generated in Russia. In this review, the actual acidic methods for alumina production (hydrochloric acid and ammonium bisulfate/sulfuric acid) were considered. Alumina powder obtained by acid methods was analyzed for the quality requirements of the Russian aluminum smelters to forward the case for the CFA's wide adoption as the raw material in both Russia's and worldwide aluminum industry.

Title: Aramid textile with near-infrared laser-induced graphene for efficient adsorption materials

Author: Cheng, J., Lin, Z., Wu, D., Liu, C., Cao, Z.

Source: 2022 Journal of Hazardous Materials

436,129150

Abstract:

Porous carbon materials show great application potential in the field of adsorption. However, the preparation process of carbon adsorption materials relies on high temperature, high energy consumption, many steps, and long time. Most of them exist in the form of powder or block, and the practical application scenarios are limited and difficult to recycle. In this study, based on in-situ carbonization of polymer precursor, we directly generated laser-induced graphene (LIG) on the surface of commercial aramid textile using a low-energy near-infrared laser in air, and prospected the application prospect of the prepared aramid/graphene textile in the field of adsorption. Under a certain laser energy, the photothermal reaction promotes the breaking of the C[dbnd]O and C[sbnd]N bonds in the surface layer of the aramid fiber, and reorganizes into a graphene structure at an instantaneous high temperature, while the overall flexible structure of the textile was not destroyed. Further, adsorption materials based on the as-prepared aramid/graphene textiles were also designed, including VOC-adsorbing textile in air and dye-adsorbing textile in water. Using low-energy near-infrared laser to directly achieve LIG writing in commercial textiles under air condition will provide an efficient, environmentally friendly, and designable direction for the large-scale fabrication of textile adsorption products.

Title: Understanding the electrochemical behavior of Sn(II) in choline chloride-ethylene glycol deep eutectic solvent for tin powders preparation

Author: Wang, Z., Cheng, M., Bu, J., (...), Hua, Y., Wang, D.

Source: 2022 Advanced Powder Technology

33(8),103670

Abstract:

Tin is one of the vital substances in the material and chemical industry. Deep eutectic solvent (DES) possesses excellent physicochemical properties for metal preparation. In this study, the electrochemical behavior of Sn(II) and metallic tin preparation in choline chloride-ethylene glycol (ChCl-EG) DES were investigated. Linear sweep voltammetry is carried out to study the effects of substrate material (Ni, Cu, Pt, C, Fe, Al, W, glassy carbon (GC) and Ti), temperature (313–353 K) and SnCl2 concentration (10–100 mM) on the electrochemical behavior of Sn(II)/Sn. Results demonstrate that metallic tin is easier to be prepared on the Ni electrode, and increasing temperature and SnCl2 concentration both facilitate the reduction of Sn(II). Electrospray ionization mass spectrometry (ESI-MS) shows that the main form of Sn(II) is [SnCl3]-. Chronoamperometric tests indicate that with the increase of applied potential, the nucleation of Sn(II) on the nickel electrode becomes close to the instantaneous nucleation. Simultaneously, the nucleation rate and the number of active sites on the electrode surface increase significantly. Pure tin with a dendritic structure could be prepared with higher current efficiency of 96.4% and lower energy consumption of 320.5 kW·h·t−1 without any additives. All these studies provide a fundamental basis for the preparation of tin powders in ChCl-EG DES.

Featured Article

Microstructure and mechanical properties of sustainable cementitious materials with ultra-high substitution level of calcined clay and limestone powder

YunxingRuan[a] TariqJamil[b] ChuanlinHu[a] Bishnu PrasadGautam[c] JingYu[d]

Highlights

- Microstructure and mechanical properties of cementitious materials with ultra-high substitution level of LCC are investigated.
- The addition of LCC is beneficial for improving the toughness of cementitious materials.
- Considering the reduction in porosity and cumulative heat release, the maximum substitution level of LCC is suggested to be 70%.

Abstract

Supplementary cementitious materials have been widely used to partially replace ordinary Portland cement. An increasing level of the substitution is a highly effective way to reduce carbon dioxide emission and energy consumption of cementitious materials. However, the availability of traditional supplementary cementitious materials (e.g., fly ash and slag) cannot meet the needs from the cement industry in the near future, particularly for the underdeveloped countries because they have limited industries with such by-products. In this study, calcined clay and limestone powder as supplementary cementitious materials are adopted to replace cement at ultra-high substitution levels for the production of sustainable cementitious materials. The influence of ultra-high substitution of calcined clay and limestone powder (i.e., from 50% to 80%) on the microstructure and mechanical properties

of cementitious materials are investigated. The results show that the addition of calcined clay and limestone powder together with 50%-70% substitution of cement is beneficial for improving the toughness, densifying the microstructure, and refining the pore structure of cementitious materials even though the compressive strength is not obviously improved. This study reveals that the key factor to affect the substitution level is the availability of portlandite in the mixture, which controls the amount of calcined clay participating in the pozzolanic reaction.

- **Previous** article in issue
- **Next** article in issue

Keywords

Sustainable cementitious materials

Limestone powder

Calcined clay

Pozzolanic reaction

Microstructure

LC3

1. Introduction

Ordinary Portland cement (OPC) is the most widely used cementitious materials [1]. However, the production of OPC is inevitably accompanied by abundant energy consumption and remarkable carbon dioxide emission [2]. The carbon dioxide emitted by global cement production accounts for 5–8% of anthropogenic carbon dioxide [2]. In line with the globally agreed sustainable development goals, a highly effective strategy to reduce the carbon footprint of the cement industry is to reduce the clinker content [3]. Replacement of cement by supplementary cementitious materials (SCMs) is the most effective solution to reduce the amount of cement clinker [4], [5], [6], [7], [8], [9]. However, at the global level, the annual supply of slag and fly ash is limited to about 15% of annual cement production [10]. Moreover, the availability of traditional SCMs is dependent on the availability of industries producing such by-products. Especially in underdeveloped countries, such industries exist in limited numbers and the reserves of traditional SCMs cannot meet the needs from the cement industry.

As a new possibility, the combination of calcined clay and limestone powder (LCC) can be treated as sustainable cementitious materials [11], [12], [13], [14], [15], [16], [17], [18]. Clay and limestone are widely distributed and abundant all over the world. The temperature for calcinating clay is generally 600–800 ℃, which is much lower than that for producing cement clinker. At 600–800 ℃, kaolinite in clay can transform to the metakaolin with pozzolanic characteristics. In addition, the combination of calcined clay and limestone can further reduce the amount of cement and enhance the formation of hydration products due to their synergistic effect. Therefore, LCC can suitably be used to partially replace cement to form limestone calcined clay cement (LC^3) and the replacement level is generally 50%, which exhibits similar mechanical properties with ordinary Portland cement at 7d [19].

Although the LC^3 reduces the content of cement clinker to 50%, further reduction of clinker can additionally contribute to the cement industry both economically and environmentally [20]. Particularly in underdeveloped countries, cheaper versions of cement blends will help to the development of infrastructure and lowing greenhouse emissions. Therefore, it is essential to determine the maximum possible level of substitution of cement with the LCC. In this study, the substitution level by LCC in the cementitious materials is increased up to 80%, and its influence on the microstructure and compressive strength of cementitious materials is investigated.

2. Materials and methods

2.1. Materials

The P.O 52.5 grade Portland cement in accordance with Chinese Standard GB175-2007, calcined clay, and limestone powder were used in this study. The oxide chemical compositions of the three raw materials were determined by X-ray fluorescence, as listed in Table 1. Their particle size distributions were investigated by laser diffraction and are shown in Fig. 1.

Table 1. Chemical composition of Portland cement, calcined clay, and limestone powder (wt. %).

Empty Cell	**CaO**	**SiO_2**	**Al_2O_3**	**Fe_2O_3**	**MgO**	**Na_2O**	**K_2O**	**CO_2**	**Others**
Portland cement	65.21	21.27	4.57	3.25	1.62	0.08	0.76	0	3.24
Calcined clay	0.03	56.79	35.63	2.00	0.34	0.20	3.49	0	1.52
Limestone powder	54.98	0.33	0.24	0.04	0.88	0	0.04	43.46	0.03

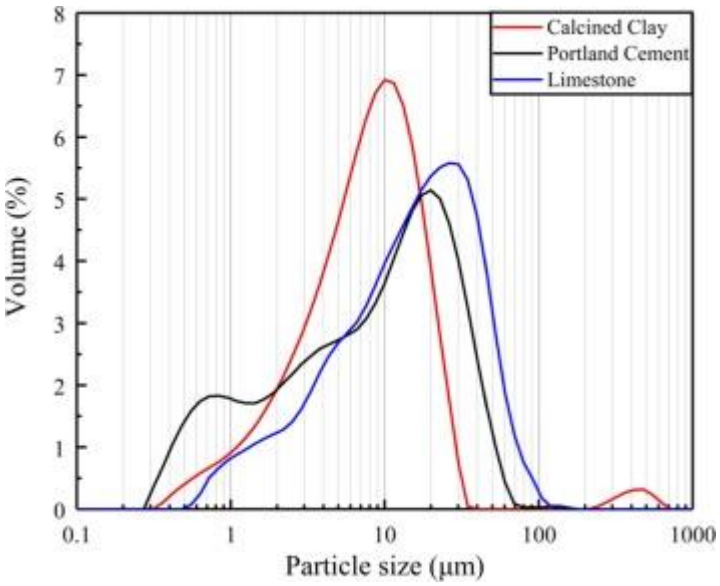

1. Download : Download high-res image (136KB)
2. Download : Download full-size image

Fig. 1. Particle size distributions of Portland cement, calcined clay, and limestone powder.

The kaolinite content of clay was determined by thermogravimetric (TG) and differential thermogravimetric (DTG) analyzes. From the TG and DTG curves in Fig. 2, the mass loss between 400 °C and 600 °C (i.e., wt\%kaol-OH) is attributed to the dehydroxylation of kaolinite [21]. Therefore, the kaolinite content of clay (wt\%kaolinite) can be calculated from the following equation [21]:(1)wt\%kaolinite=wt\%kaol-OHMkaolinite2Mwaterwhere Mkaolinite is the molecular mass of kaolinite (i.e., 258) and Mwater is the molecular mass of water (i.e., 18). As shown in Fig. 2, the mass loss due to the dehydroxylation of kaolinite was 6.97%. Thus, the kaolinite content of clay used in this study was determined to be 50% according to Eq. (1).

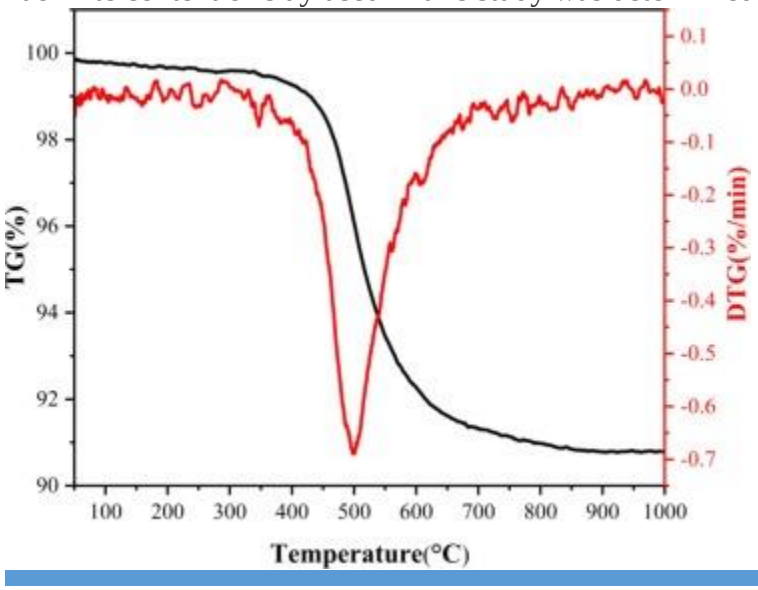

1. Download : Download high-res image (111KB)
2. Download : Download full-size image

Fig. 2. TG and DTG curves of clay.

2.2. Sample preparation

In this study, the calcined clay to limestone powder mass ratio in LCC was fixed as 2 according to the recommendation in a previous study [19], while the substitution level by LCC was increased in increments of 10% from 50% to 80% and two different water to binder ratio (w/b = 0.5 and 0.4) were set. The mix proportions adopted in this study are listed in Table 2. The label LCC*X*-*Y* represents that the content of the calcined clay and limestone powder is *X* % (wt. %) of the binder and the water to binder ratio is *Y*. For example, LCC50-0.5 represents that the calcined clay and limestone powder occupy 50% of the binder and the water to binder ratio is 0.5. Moreover, a commercial superplasticizer (SP) with solid content of 16% was used to make sure that all samples had similar fluidity. Similarly, 2% gypsum was added to all the blended cement samples, particularly considering the relatively high content of calcined clay and limestone powder. While the content of gypsum blended in OPC varied with a variation in cement content, the content of added gypsum was kept constant for all mixes. It should be noted that the additional 2% gypsum in the mix caused the cement content in the overall mix to reduce by 2%.

Table 2. Mix proportions.

Label	Cement	Calcined Clay	Limestone powder	Gypsum	w/b
LCC50-0.5	48%	33.33%	16.67%	2%	0.5
LCC50-0.4	48%	33.33%	16.67%	2%	0.4
LCC60-0.5	38%	40.00%	20.00%	2%	0.5
LCC60-0.4	38%	40.00%	20.00%	2%	0.4
LCC70-0.5	28%	46.67%	23.33%	2%	0.5
LCC70-0.4	28%	46.67%	23.33%	2%	0.4
LCC80-0.5	18%	53.33%	26.67%	2%	0.5
LCC80-0.4	18%	53.33%	26.67%	2%	0.4
Cement	100%	0	0	0	0.4

In order to prepare the paste mixture, the raw materials were dry mixed in the mixer for 1 min to ensure uniformity. Then, water with superplasticizer was added into the mixer and the resulting

mixture was mixed for another 3 min. After that, the paste mixture was cast into the molds with the size of 40 mm ×40 mm ×160 mm, sealed by plastic wraps, and placed in a room at a temperature of 20 ± 2 °C for 1 d before demolding. After being demolded at 1 d, the hardened cement paste specimens were cured in a room with relative humidity close to 100% and the temperature of 20 ± 2 °C until they were tested at the ages of 3 d, 7 d, and 28 d.

2.3. Characterization methods

The compressive strength and flexural strength of the hardened cement paste specimens were measured by a compression testing machine. The flexural strength test was performed by maintaining a span of 100 mm in a three-point bending test. The loading rates of the compressive test and the flexural test were 1 kN/s and 0.5 kN/s, respectively. After the flexural and compressive tests, the central parts of the samples were immediately submerged in isopropanol to terminate their hydrations and then subjected to the following characterizations.

X-ray diffraction (XRD) patterns of the samples were measured by an X-ray diffractometer (Empyrean, Germany). The quantification of the phases was obtained through the Rietveld-XRD analysis, and α-Al_2O_3 was added as the standard material. The 28d samples were subjected to a slow scan rate of 2 deg./min in the range of 5°-25°.

The mercury intrusion test was performed by using Mike Auto Pore IV 9500 high-performance automatic mercury intrusion meter.

TAM Air calorimeter (C80, SETARAM, France) was adopted to monitor the heat release rate and cumulative heat release of the samples, where the temperature was kept at 20 °C.

The microstructures of the samples were characterized by a scanning electron microscope (SEM, QUANTA FEG450) and the operating voltage was chosen as 15 kV.

3. Results and discussion

3.1. Strength development

The compressive strengths of the samples are summarized in Fig. 3. For all test ages expect 1d, compressive strength gradually decreased with an increase in the proportion of calcined clay and limestone powder in the binder from 50% to 80%. In addition, when the water to binder ratio gradually decreased from 0.5 to 0.4, the compressive strength gradually increased as expected

for hardened cement paste specimens. The compressive strengths of all LCC specimens were lower compared to the cement paste (denoted as "Cement" in the figures) at 1 d, while the compressive strength of LCC50 increased rapidly after 3 d and the compressive strength was close to the cement paste at 7 d. In addition, for the LCC with higher substitution levels, e.g., LCC70 and LCC80, the compressive strengths increased before 7 d, while the increase of compressive strength became much slower from 7 d to 28 d. This is attributed to a large amount of unreacted calcined clay and limestone powder that acted as filler, and thus they had barely any contribution to impart the strength of LCC.

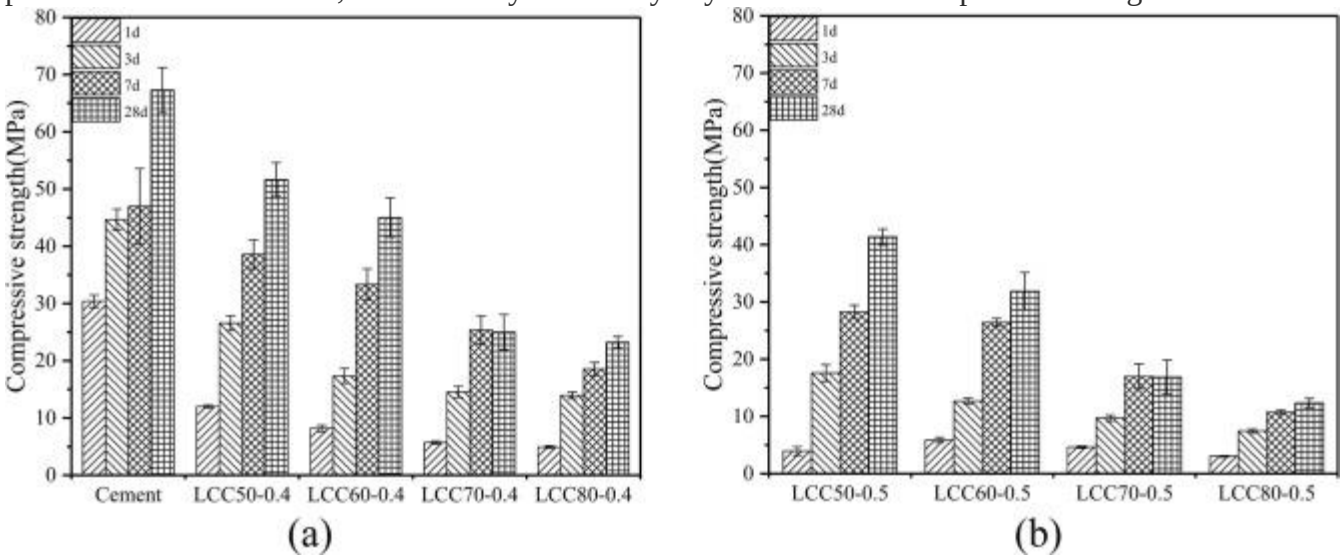

1. Download : Download high-res image (446KB)
2. Download : Download full-size image

Fig. 3. Compressive strengths of LCC50, LCC60, LCC70, LCC80 and cement paste at the age of 1, 3, 7, and 28 d and different w/b: (a) w/b = 0.4, (b) w/b = 0.5.

The flexural strengths of the different limestone-calcined clay cement blends are summarized in Fig. 4. The trend of development of the flexural strengths of LCC specimens was consistent with the development of their respective compressive strengths. The flexural strength of LCC50 was close to that of cement paste at 28 d. The flexural to compressive strength ratio of LCC50, LCC60, LCC70, and cement paste at 1, 3, 7 and 28 d with w/b is 0.4 are summarized in Fig. 5. The flexural to compressive strength ratios of LCC were higher than that of cement paste, indicating that the addition of calcined clay and limestone powder was beneficial to improving the toughness of cementitious materials.

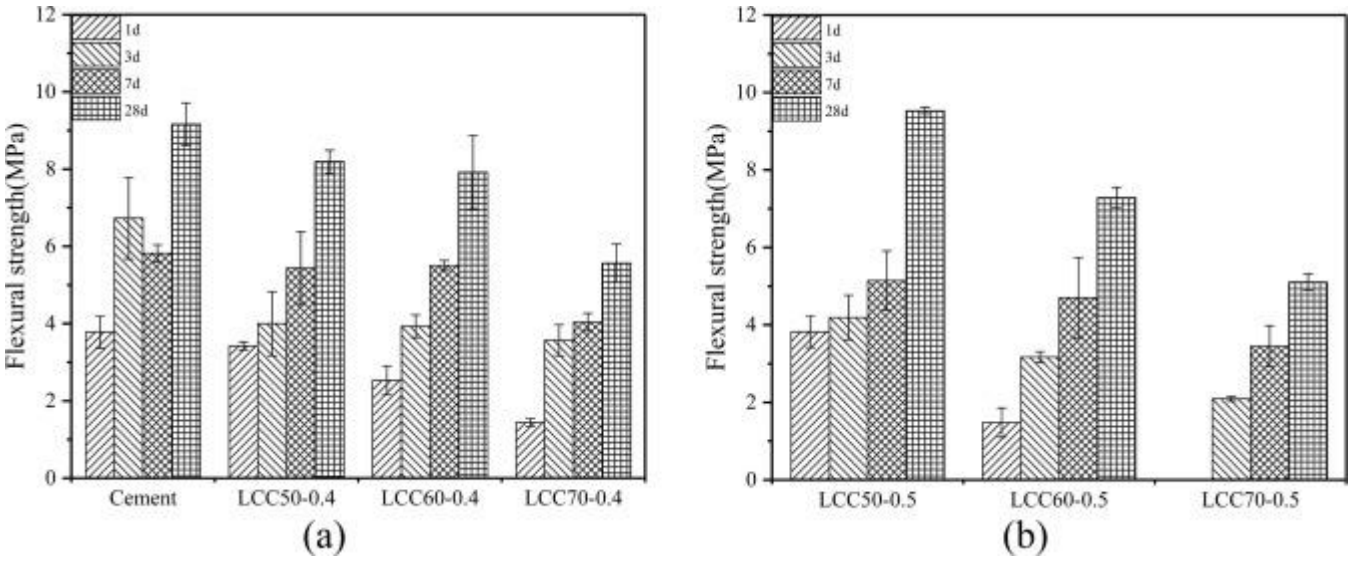

1. Download : Download high-res image (572KB)
2. Download : Download full-size image

Fig. 4. Flexural strengths of LCC50, LCC60, LCC70, LCC80 and cement paste at the age of 1, 3, 7, and 28 d and different w/b: (a) w/b = 0.4, (b) w/b = 0.5.

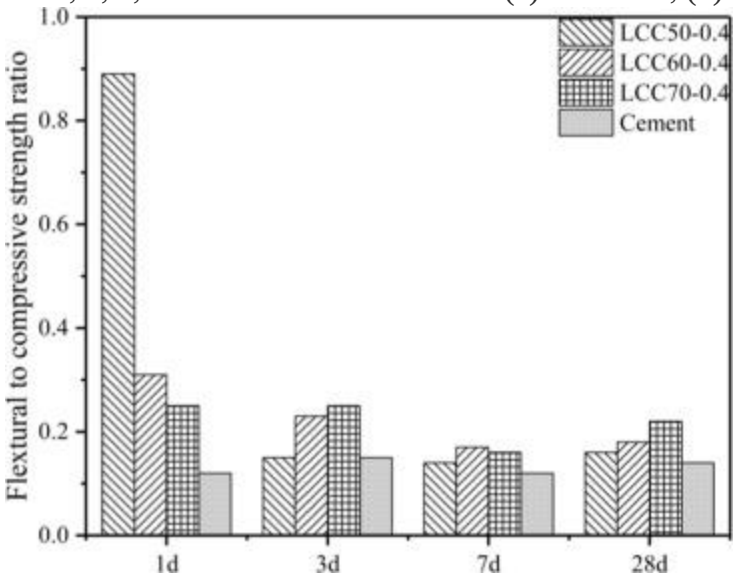

1. Download : Download high-res image (150KB)
2. Download : Download full-size image

Fig. 5. The flexural to compressive strength ratio of LCC50, LCC60, LCC70, and cement paste at ages of 1, 3, 7 and 28 d at w/b of 0.4.

3.2. Hydration products

The evolution of the ettringite (AFt), carboaluminate (Hc + Mc) and calcium hydroxide (CH) of LCC specimens at w/b of 0.4 was obtained by Rietveld-XRD refinement, as shown in Fig. 6. The content of CH gradually decreased with the age in LCC50 and LCC60, and more C-A-S-H gel were formed, which is attributed to the pozzolanic reaction between calcined clay and calcium hydroxide generated from cement hydration [19]. So, the compressive strengths of the LCC50 and LCC60 increased markedly at later ages. However, the CH content disappeared of LCC70 and LCC80 after 7 d, indicating that the calcium hydroxide had been completely consumed before 7 d. Therefore, in LCC70 and LCC80 after 7 d, no enough calcium hydroxide was available to react with the calcined clay, resulting in lower amount of calcined clay that participated in the pozzolanic reaction, and the slow development of strength at later ages. The content of carboaluminate phases, i.e., hemicarboaluminate (Hc) and monocarboaluminate (Mc), increased significantly with the age in LCC specimens except LCC80, because the limestone powder could react with aluminate phase to form carboaluminate phases [22]. It can be observed that the content of carboaluminate gradually decreased as the content of calcined clay and limestone increases, indicating smaller amount of limestone powder participating in the reaction at higher substitution level. The content of ettringite fluctuated with the increase of age, but it still stably existed in the LCC systems at 28d. In the case of cement system without limestone powder, ettringite is easily transformed into monosulphoaluminate, but this transformation is prevented when limestone powder is present [23], [24], so that ettringite can be stabilized in the LCC systems [25], [26], [27], [28].

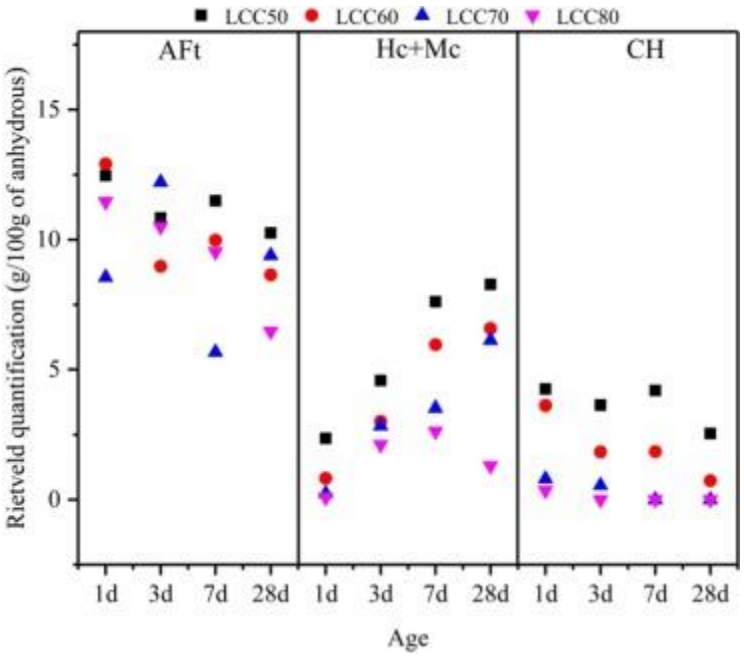

1. Download : Download high-res image (96KB)
2. Download : Download full-size image

Fig. 6. Rietveld quantification of AFt, Hc + Mc and CH in the LCC specimens at w/b of 0.4 and ages of 1, 3, 7 and 28 d.

Fig. 7 shows XRD patterns of LCC50, LCC60, LCC70, LCC80 and cement paste with different w/b at age of 28 d. The CH peak appeared sharply in OPC, but became weak in LCC50 and LCC60 and disappeared in the higher content of calcined clay and limestone system, which should be attributed to the pozzolanic reaction of calcined clay. Diffraction peaks of ettringite were observed in all LCC systems, but only weak ettringite diffraction peaks were present in OPC, which can be explained by ettringite converting to monosulfate. Moreover, all LCC systems showed the diffraction peak of carboaluminate, because of the limestone in LCC as the source of carbonate.

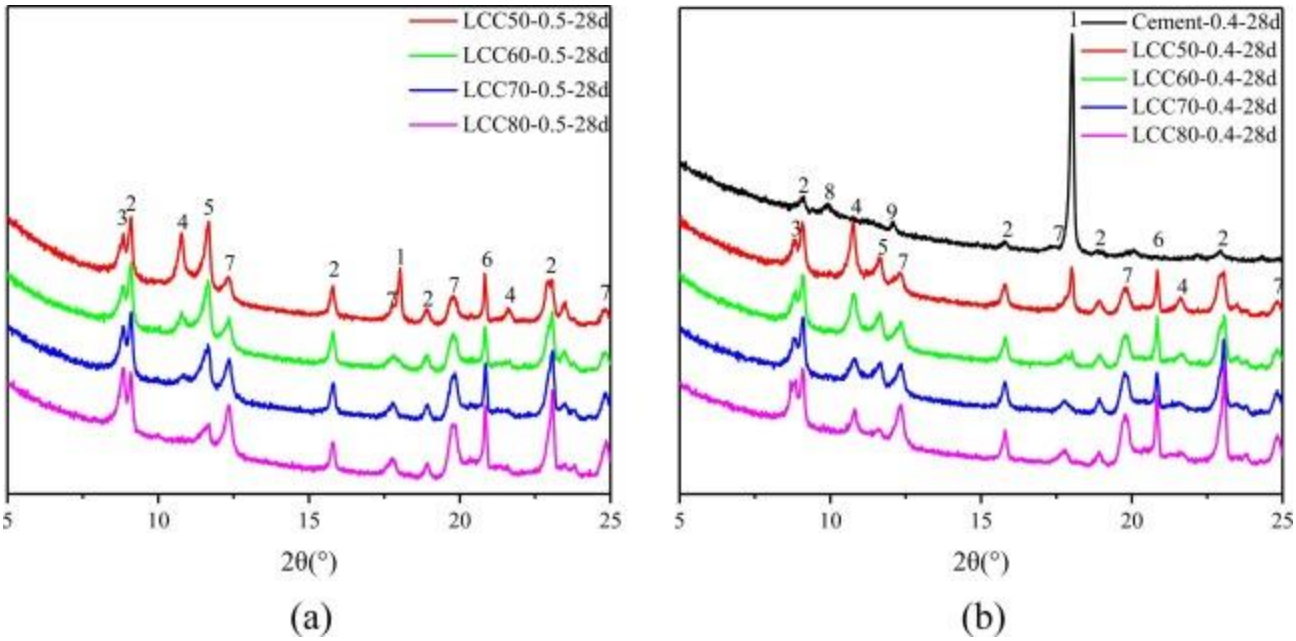

1. Download : Download high-res image (392KB)
2. Download : Download full-size image

Fig. 7. XRD patterns of LCC50, LCC60, LCC70, LCC80 and cement paste at the age of 28d and different w/b: (a) w/b = 0.5, (b) w/b = 0.4 (1-Portlandite 2-Ettringite 3- Muscovite 4-Hemicarboaluminate 5- Monocarboaluminate 6- Quartz 7-Kaolinite 8-Monosulfate 9-C_4AF).

3.3. Isothermal calorimetry

The heat release curves of all LCC systems and cement paste are shown in Fig. 8. The heat release peak of cement paste is a single peak, which is mainly contributed by the hydration of C_3S. Obvious double peaks can be seen in the LCC systems, where the first peak is the exothermic peak of silicate phase hydration, and the second peak is the exothermic peak of aluminate phase hydration [29]. In addition, the induction period of LCC systems was advanced compared to cement paste. The first exothermic peak of cement paste hydration occurred at 12 h and the first exothermic peak of LCC occurred around 8 h. This might be because the addition of calcined clay and limestone powder had "filler effect" and accelerated the hydration of cement clinker [30], [31], [32]. Furthermore, with an increase in substitution, the "filler effect" becomes more prominent, resulting that the first exothermic peak appeared earlier and higher when w/b was 0.5 (Fig. 8a). But this phenomenon was not reflected when the water to binder ratio was 0.4, since more SP was added at low w/b in order to maintain a consistent workability, the increased SP dosage retarded the hydration reaction and delayed the appearance of the exothermic peak [33]. Moreover, the "filler effect" of calcined clay and limestone

powder accelerated the hydration of cement clinker, and the addition of calcined clay provided supplementary aluminate phase, which affected the second exothermic peak. Therefore, the second peak was enhanced and appeared in advance with the increase of the content of calcined clay and limestone in LCC systems. According to the cumulative heat release curves in Fig. 8, the cumulative heat release per gram of cement in the cement specimen was less than that in LCC systems, which also showed that the addition of calcined clay and limestone was beneficial to cement hydration, and the effect of promoting cement hydration was more obvious with an increase in substitution level.

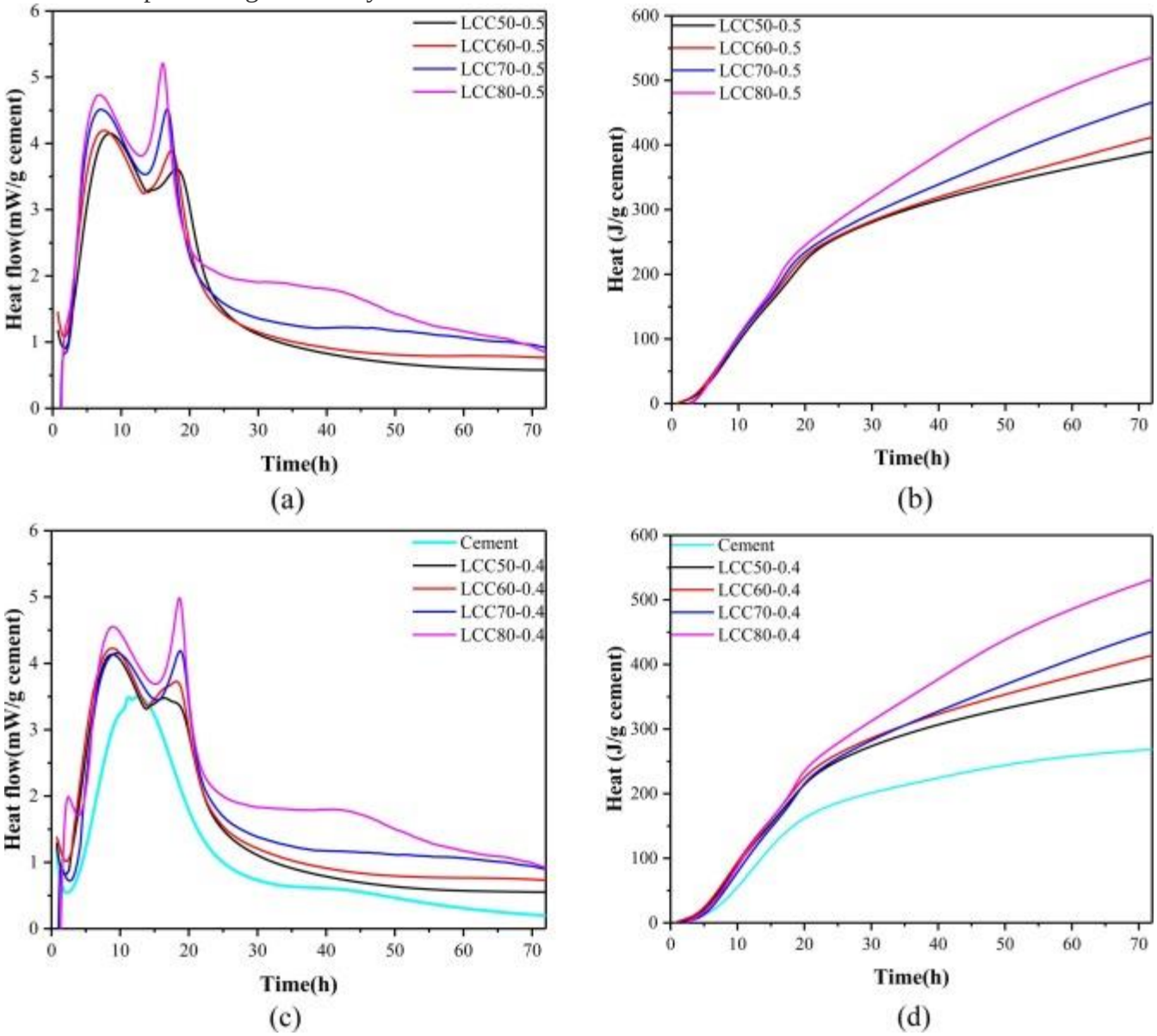

1. Download : Download high-res image (532KB)
2. Download : Download full-size image

Fig. 8. Heat release curves and cumulative heat release curves of LCC50, LCC60, LCC70, LCC80 and cement paste under different w/b: (a-b) w/b = 0.5, (c-d) w/b = 0.4.

3.4. Microstructure

Based on the above analyses, C-A-S-H gels, ettringite, hemicarboaluminate and monocarboaluminate are the main hydration products in the LCC systems, which help to improve the porosity and form dense microstructure. The SEM images of the samples at age of 28d and w/b of 0.4 are shown in Fig. 9. Compared with LCC70 and LCC80 systems, a large number of carboaluminate phases (Fig. 9a) and C-A-S-H gel spots (Fig. 9b) were clearly observed in LCC50 and LCC60. Furthermore, the presence of ettringite was observed in LCC80, which further showed that ettringite can stably exist in the LCC system with 80% substitution level. Calcium hydroxide was not observed in the LCC systems due to its consumption by pozzolanic reaction, while calcium hydroxide could be clearly observed in cement paste.

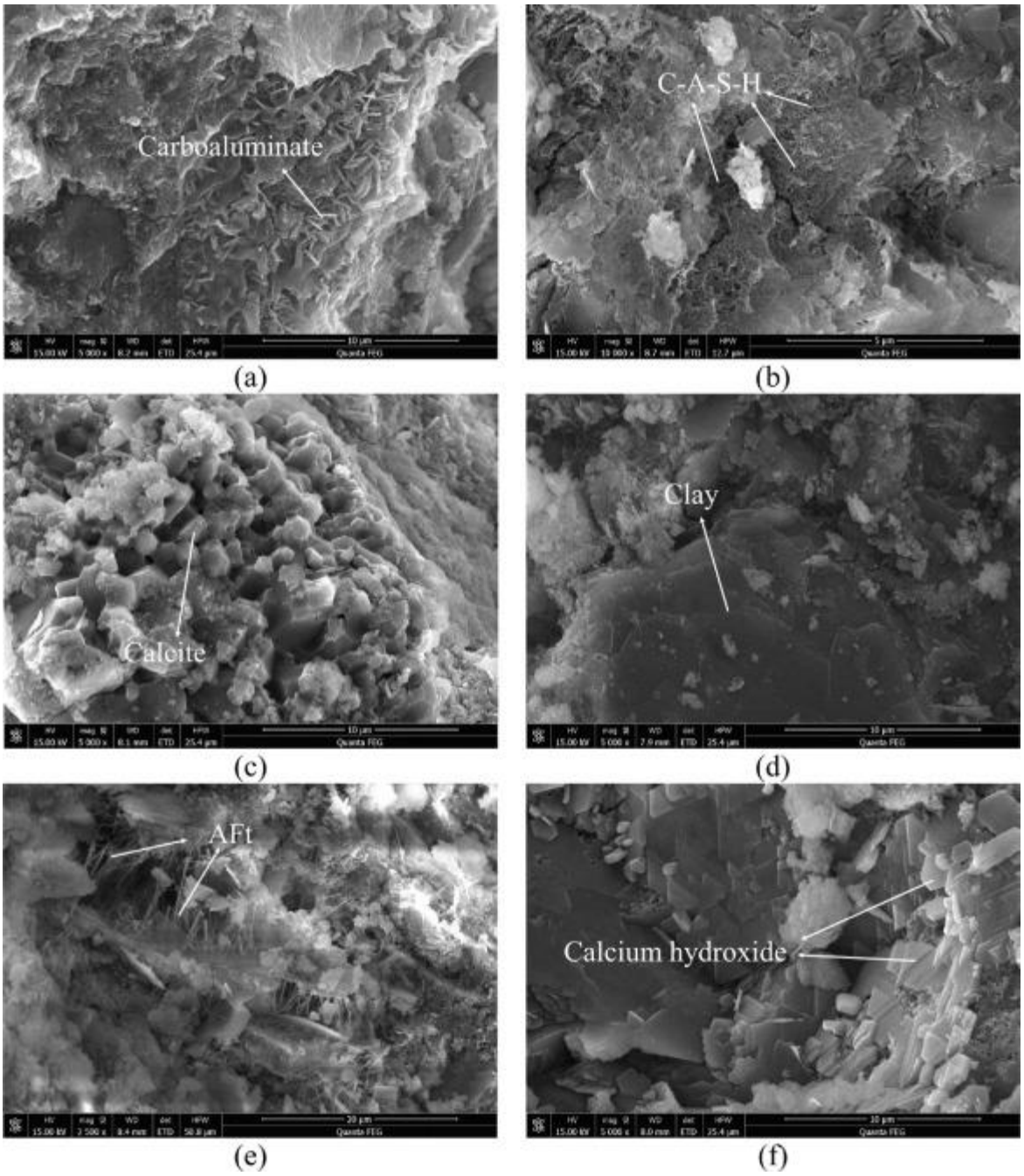

1. Download : Download high-res image (1MB)
2. Download : Download full-size image

Fig. 9. SEM images of (a) LCC50, (b) LCC60, (c) LCC70, (d-e) LCC80 and (f) cement paste at age of 28d with w/b of 0.4.

Fig. 10 shows the cumulative porosity curves and pore size distribution curves of LCC50, LCC60, LCC70, LCC80, and cement paste at 28d. The pores of cement-based materials can be divided into

capillary pores (including large pores ranging from 50 nm −10 μm and medium pores ranging from 10 nm −50 nm), gel pores (ranging from 2.5 nm to 10 nm) and interlayer pores (<0.5 nm) [34]. The pore structure could remarkably influence the durability and the mechanical properties of cement-based materials. Fig. 10 shows that the cumulative porosity of LCC were higher than that of cement paste, and the cumulative porosity gradually increased with an increase in substitution level. However, the pore sizes at the peaks of pore size distribution of LCC50, LCC60, and LCC70 were smaller than that of cement paste, while the pore size at the peak of LCC80 was suddenly increased and became larger than that of cement paste. On the other hand, the pore size ranges of LCC50 and LCC60 were narrow and distributed mainly in the range of gel pores that were generally regarded as innocuous to the strength. Due to the synergistic effect of calcined clay and limestone in LCC, additional hydrated products such as C-A-S-H gel, ettringite and carboaluminate were continuously formed, which helped to fill and refine the pores, making a denser microstructure. However, when the substitution level was too high (80%), the cumulative porosity of LCC was larger than that of cement paste and the pore size range became wider, which was consistent with the insufficient reaction and the low compressive strength as explained in section 3.1. The pore size distribution curves of the LCC system were single-peak (Fig. 10), while that of the cement paste has two separate peaks, indicating that the pore size distribution of the LCC system was concentrated in the fine pores.

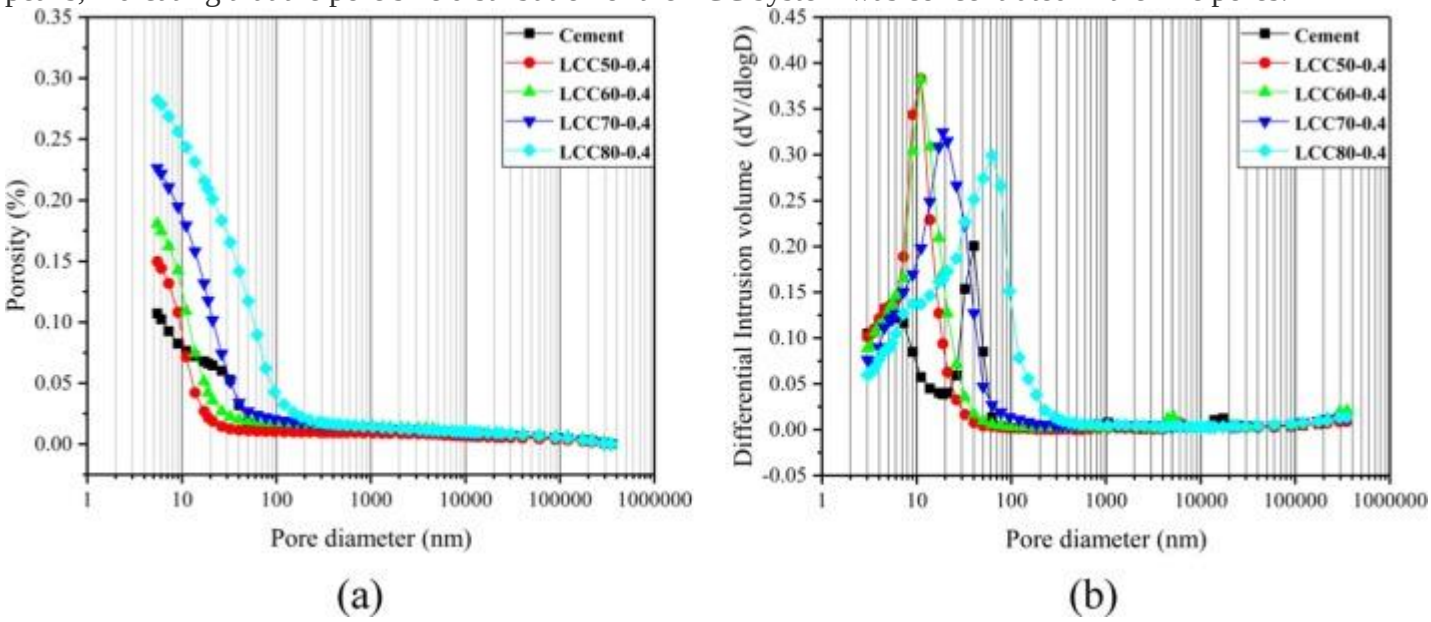

1. Download : Download high-res image (356KB)
2. Download : Download full-size image

Fig. 10. (a) Cumulative porosity curves and (b) pore size distribution curves of LCC50, LCC60, LCC70, LCC80, and cement paste at age of 28d and w/b of 0.4.

4. Conclusions

In this study, the substitution level of cement by calcined clay and limestone powder (LCC) was gradually increased from 50% to 80%, and the influence of this approach on the microstructure and mechanical properties of cementitious materials was comprehensively investigated by various techniques. Following conclusions can be drawn:

(1)

The compressive strengths of the LCC50 and LCC60 systems are lower than that of cement paste at 1 and 3 d, while they increase faster from 3 to 7 d. The compressive strength of LCC system with higher substitution level (i.e., LCC70 and LCC80, increases slowly at later age (from 7 to 28 d). The flexural strength development of LCC has the same trend as the compressive strength development. However, the flexural to compressive strength ratio of LCC (up to 70% substation) is higher than that of cement paste, indicating that the addition of LCC is beneficial for improving the toughness of cement-based materials.

(2)

The amount of carboaluminate increases with the age due to the synergistic effect of the calcined clay and limestone powder, while the content of calcium hydroxide gradually decreases. After 7 d, calcium hydroxide disappears in LCC70 and LCC80, indicating that the calcium hydroxide is quickly consumed by the calcined clay. The result shows that portlandite in the LCC with high substitution level is weak, resulting in the lower amount of calcined clay that participates in the reaction.

(3)

The induction period of LCC becomes shorter than that of cement paste at w/b of 0.5 and 0.4 due to the filler effect of calcined clay and limestone powder. In addition, with the increase in substitution level, the filler effect of calcined clay and limestone powder becomes more obvious and the induction period of LCC becomes shorter.

(4)

The cumulative porosity of the LCC is higher than that of cement paste, and the cumulative porosity gradually increases with an increase in substitution level. However, pore sizes at the peaks of LCC50, LCC60, and LCC70 are smaller than that of cement paste. The pore size ranges of LCC50 and LCC60 are very narrow and distributed mainly in the range of gel pores, while the pore size at the peak of LCC80 increases suddenly.

(5)

Considering the reduction in porosity and cumulative heat release, the maximum possible level of substitution of cement with LCC is obtained as 70% even though compressive strength is reduced by 48% at w/b of 0.4 compared to the 50% substitution level. Further studies are required to improve the compressive strength and to expand the engineering application of sustainable cementitious materials with ultra-high substitution level of LCC.

CRediT authorship contribution statement

Yunxing Ruan: Investigation, Data curation, Writing – original draft. **Tariq Jamil:** Writing – review & editing. **Chuanlin Hu:** Supervision, Writing – review & editing, Conceptualization, Funding acquisition. **Bishnu Prasad Gautam:** Writing – review & editing. **Jing Yu:** Writing – review & editing, Conceptualization, Funding acquisition.

https://www.sciencedirect.com/science/article/pii/S0950061821031561

References

RUAN, Y., JAMIL, T., HU, C., GAUTAM, B. P. AND YU, J.

Microstructure and mechanical properties of sustainable cementitious materials with ultra-high substitution level of calcined clay and limestone powder. Ruan, Y., Jamil, T., Hu, C., Gautam, B. and Yu, J., 2022. Microstructure and mechanical properties of sustainable cementitious materials with ultra-high substitution level of calcined clay and limestone powder. [online] Available at: <https://www.sciencedirect.com/science/article/pii/S0950061821031561> [Accessed 25 July 2022].

Ruan, Y., Jamil, T., Hu, C., Gautam, B. and Yu, J., 2022. Microstructure and mechanical properties of sustainable cementitious materials with ultra-high substitution level of calcined clay and limestone powder. [online] Available at: <https://www.sciencedirect.com/science/article/pii/S0950061821031561> [Accessed 25 July 2022].

https://www.copper.org/resources/properties/129_6/